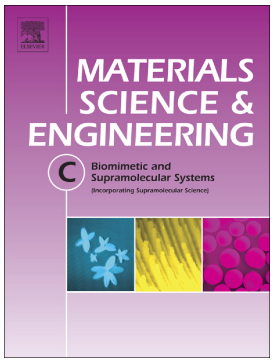

A comparative in vivo evaluation of bioactive glasses and bioactive glass-based composites for bone tissue repair

Devis Bellucci, Alexandre Anesi, Roberta Salvatori, Luigi Chiarini, Valeria Cannillo

PII: S0928-4931(17)31309-7
DOI: doi: 10.1016/j.msec.2017.05.062
Reference: MSC 8044

To appear in: *Materials Science & Engineering C*

Received date: 7 April 2017
Revised date: 26 April 2017
Accepted date: 10 May 2017

Please cite this article as: Devis Bellucci, Alexandre Anesi, Roberta Salvatori, Luigi Chiarini, Valeria Cannillo , A comparative in vivo evaluation of bioactive glasses and bioactive glass-based composites for bone tissue repair, *Materials Science & Engineering C* (2017), doi: 10.1016/j.msec.2017.05.062

A comparative in vivo evaluation of bioactive glasses and bioactive glass-based composites for bone tissue repair

Devis Bellucci[1*], Alexandre Anesi[2], Roberta Salvatori[2], Luigi Chiarini[2] and Valeria Cannillo[1].

[1] Department of Engineering "E. Ferrari", University of Modena and Reggio Emilia, Via P. Vivarelli 10, 41125 Modena, Italy.

[2]Lab. Biomaterials, Department of Medical and Surgical Sciences of Children & Adults, University of Modena and Reggio Emilia, Via Campi 213/A, 41125 Modena, Italy.

[*] Corresponding-Author: Dr. Devis Bellucci,

Department of Engineering "E. Ferrari", University of Modena and Reggio Emilia, Via Vignolese 905, 41125 Modena, Italy

Telephone: +39-059-2056233; fax: +39-059-2056243; e-mail: devis.bellucci@unimore.it

Abstract

In this work a set of novel materials for bone tissue regeneration have been tested *in vivo* in an animal model. In fact, despite many studies have been devoted to amorphous 45S5 Bioglass®, there is lack in the literature of works aimed to study the *in vivo* performance of heat-treated – and thus partially crystallized – 45S5. As widely reported, crystallization limits the bioactivity of 45S5 and is the main reason that prevents a broader use of this material. Thus, in the present work, a recently developed bioactive glass (BG_Ca/Mix) is tested, since previous investigations demonstrated that BG_Ca/Mix is particularly promising by virtue of both its high bioactivity and lower tendency to crystallize with respect to 45S5. BG_Ca/Mix sintered powders and two composites, which contain BG_Ca/Mix and an increasing percentage (20 wt.% or 70 wt.%) of hydroxyapatite (HA), were considered. As a term of comparison, 45S5 sintered powders were also studied. The samples were implanted in rabbits' femurs and harvested after 8 weeks. The histological analysis demonstrated that BG_Ca/Mix has an osteoconductive ability slightly higher than that of 45S5 glass-ceramics, followed by that of the composites, which may represent the starting point for obtaining systems with degradation rate tailored for a given clinical application. Moreover, the 45S5 samples were locally cracked, probably because of a non-uniform dissolution in the physiological environment. On the contrary such cracks, which could lead to implant instability and unsuitable mechanical performance, were not observed in BG_Ca/Mix.

Keywords: Bioactive glasses; Composites; Osteoconductivity; In vivo models; Bone regeneration.

1. Introduction

The biomaterials field has grown significantly over the last 50 years, evolving through three different generations: biointert materials (first generation), bioactive and biodegradable materials (second generation) and, finally, materials designed to induce appropriate responses at the molecular level (third generation) **[1]**. Recent developments include hybrid and inorganic materials for delivery, therapy, sensors, etc **[2–5]**; nanoparticles for drug and gene delivery **[6 – 8]**, metal nanostructures for photothermal therapy **[9, 10]**, systems with antibacterial and anti-inflammatory properties **[8, 11, 12]**, functionally graded materials **[13]**, advanced bio-coatings **[14–15]**, tissue and bone substitutes **[16, 17]**. In this context, the pathologies associated with the musculoskeletal system involve hundreds of millions of people all over the world. The need for new surgical materials to treat musculoskeletal infirmities and, in particular, bone loss due to cancer, trauma, osteoporosis and jaw atrophies, has focused the interest of materials' scientists on calcium phosphate ceramics (CPs), which currently play a fundamental role in orthopaedics, hand surgery, maxillofacial and oral surgery **[18, 19]**. In fact, thanks to their high biocompatibility, CPs are ideal candidates for the realization of prostheses, orthopaedic devices and synthetic bone grafts. Among CPs, hydroxyapatite (HA) is probably the most widely used material, by virtue of its close crystal and chemical resemblance to the inorganic component of biological hard tissues (*i.e.*, bone and teeth). In fact, HA is highly osteoconductive and it is able to form a strong bond with the surrounding living bone **[20]**.

Bioactive glasses are an attractive alternative to HA, as they are typically able to bond to bone more rapidly than other bioceramics. 45S5 Bioglass® **[21]**, a degradable glass in the $Na_2O–CaO–SiO_2–P_2O_5$ system, was the first bioactive glass discovered. Bioactive glasses have unique properties, if compared to CPs and HA. In addition to their high reactivity *in vivo*, *in vitro* studies reported that the ions released during the 45S5 Bioglass® dissolution (e.g. Si, P, Ca) seem to induce angiogenesis, neo vascularisation and stimulate

osteoblasts proliferation and new bone growth **[22]**. Moreover, certain compositions of bioactive glasses are able to bond to both bone and soft connective tissues **[23]**.

Probably, the main disadvantage of Bioglass® and, in general, of bioactive glasses, is their tendency to crystallize during the heat treatments which are necessary for the production of special products, such as scaffolds, coatings and composites with CPs as second phase. In fact, crystallization may reduce the bioactivity of the final system **[24]**. For these reasons, the investigation of new bioactive glasses with low tendency to devitrification, to be used whenever a heat treatment is necessary, is particularly important. Among such novel compositions, the so-called BG_Ca/Mix (47.3 mol% SiO_2, 45.6 mol% CaO, 2.3 mol% K_2O, 2.3 mol% Na_2O, and 2.6 mol% P_2O_5) **[25, 26]**, which has been developed in recent years, looks particularly promising: while a crystallization temperature of about 650 °C is reported for Bioglass® **[27]**, BG_Ca/Mix starts to crystallize at temperatures as high as 880 °C. Moreover, BG_Ca/Mix is characterized by a slower ion leaching in physiological solution with respect to Bioglass®, thus determining pH values which can be considered optimal for cell adhesion, proliferation and differentiation **[25]**.

In previous works, BG_Ca/Mix have been successfully used to deposit coatings and, in particular, for the realization of HA-based composites containing up to 80 wt.% of glass **[28–30]**. The production of HA/bioactive glass composites is especially interesting, as it is possible to overcome the intrinsic limits of the glassy and the ceramic phases when considered singularly. The main objective is to tailor the biodegradation rate and the bioactivity of the resulting system by varying the volume fractions of the two constituents. Moreover, the use of bioactive glasses can be exploited to incorporate ions of biological interest within HA lattice, such as silicon, strontium, magnesium, etc, in order to simulate the behaviour of the so-called biological apatite, *i.e.* the mineral part of bone, which is typically nonstoichiometric and characterized by several ionic substitutions **[18, 31]**. Thanks to the peculiarities of BG_Ca/Mix, it was possible to sinter the HA-based composites at lower temperatures with respect to samples with the same HA/Bioglass® ratio, thus reducing the crystallization of the glassy phase and avoiding the decomposition of HA and/or reactions between HA and glass. The *in vitro* biocompatibility of both

BG_Ca-Mix and of HA/BG_Ca-Mix composites has been successfully proved in recent investigations **[28, 32]**.

In the present work, for the first time, the novel BG_Ca/Mix (sintered powders) and the HA/BG_Ca-Mix composites have been tested *in vivo* in an animal model. The samples were implanted bilaterally in the midshafts rabbit femurs and harvested after 8 weeks. Two composites with an increasing content of HA were considered. It should be noted that, although the literature reports several studies dealing with HA-based composites with phosphate bioglasses as second phase, only in the last years silicate glasses, such as Bioglass®, have been employed in combination with HA to realize biocomposites, by virtue of their osteoinductivity. Therefore, in the literature, there is lack of investigations dealing with these systems and based on animal models. Furthermore, in this work also 45S5 sintered powders were implanted and considered as a term of comparison. In fact, the *in vivo* behaviour of 45S5-derived glass ceramics is fundamental in order to evaluate the feasibility of specific implants, such as 45S5 scaffolds, whose production may require the consolidation of glass powders. Although in the last 40 years innumerable studies have been devoted to amorphous 45S5 **[24, 33]**, only in recent years the efforts of several researches have been addressed to understand the connections between sintering, crystallization and *in vivo* bioactivity of heat-treated 45S5.

2. Materials and Methods

2.1 Bioactive glasses and Composites preparation

Bioactive glass powders were produced by melting the commercial raw materials (SiO_2, $Ca_3(PO_4)_2$, $CaCO_3$, Na_2CO_3, all reagent grade - Carlo Erba Reagenti, Italy; to prepare BG_Ca/Mix, part of Na_2CO_3 has been replaced by K_2CO_3) in Pt crucibles at 1450°C. The following thermal cycle was employed: from room temperature to 1100 °C at 10 °C/min; an isothermal step at 1100 °C for 1 h to allow decarbonation; from 1100 °C to 1450 °C at 10 °C/min. The molten glasses were quenched into water to obtain two frits, which have been left to dry in an oven at 110°C for 24 hours. The 45S5 and BG_Ca/Mix frits have been

subsequently crushed in dry conditions in a porcelain jar and finally sieved to obtain a powder (grain size < 67 μm). Subsequently, 45S5 and BG_Ca/Mix powders were wetted with acetone and pressed to produce green bodies. As previously reported in Refs **[25, 34]**, 45S5 and BG_Ca/Mix green bodies were sintered for 3 h at 1050°C and 800°C, respectively. A heating rate of 10°C/min was used for both glasses. At the end of the thermal treatments the samples have been extracted from the oven and left to cool down at room temperature.

The BG_Ca/Mix glass powders were mixed with commercial HA powders (CAPTAL® Hydroxylapatite, Plasma Biotal Ltd, UK) for 6 h in a polyethylene bottle using a roll shaker to obtain the following set of composites:

- 80 wt.% BG_Ca/Mix and 20 wt.% HA powders ("80BG20HA");
- 30 wt.% BG_Ca/Mix and 70 wt.% HA powders ("30BG70HA").

80BG20HA and 30BG70HA powders were then wetted with acetone and pressed to produce the green bodies, which have been heat-treated for 3 h at 830°C and 900°C, respectively, as reported in previous works **[28]**. Finally, the fully dense bodies (45S5, BG_Ca/Mix and composites) were abraded to obtain samples in form of prismatic rods (~6x2x2 mm), which were subsequently sterilized in ethylene oxide before implantation.

2.2 Animals and surgery

Eight healthy six-months-old white New Zealand rabbits (Harlan Laboratories S.r.l., Correzzana, Monza e Brianza, Italy) with an average body weight of 5,00 kg were used. The animals were maintained for acclimation to housing conditions with food and water *ad libitum* at least for one week before surgery. The night before surgery, each animal was fasted to be ready for anaesthesia. The experiments were carried out according to the Bioethical Committee of the Italian National Institute of Health and authorized with Decrees of the Italian Ministry of Health (Protocol Number: 210/2013-B). Animal care, maintenance, and surgery were conducted in accordance with Italian law (D.L. n°. 26/2014) and European legislation (EEC n°. 63/2010).

The animals were weighed and submitted to the same surgical procedure under general anesthesia with a mixture of xylazine (4 mg/kg body weight) (Sedaxylan®, Dechra

Veterinary Products S.r.l., Turin, Italy) and ketamine (30 mg/kg body weight) (Imalgene 1000®, Merial Italia S.p.A., Milan, Italy). If necessary, further sedation was obtained by means of propofol (7 mg/kg) (Propovet®, Ecuphar S.r.l., Piacenza, Italy) administrated in the marginal ear vein.

After induction of anesthesia, shaving and antisepsis were carried out on the legs to be operated. A 3 cm long skin incision was made on the antero-lateral surface of the tight; after blunt dissection of muscles, the proximal diaphysis of the femur was reached. An incision was made on the periosteum by a scalpel to expose the femur cortex. Two cortical holes of 3.5 mm in diameter and 7 mm in depth in the midshafts rabbit femur were bilaterally drilled under continuous saline irrigation, using a bone trepan bur (227B.204.040; Komet Italia S.r.l., Milan, Italy; motor system and drilling procedure: run at a speed of 1700 rpm, Physiodispenser 7000, Nouvag AG; Switzerland).

Three rods of different bioactive glass/composite and one sham (without implant) were placed in the left and right femur of each rabbit, as shown **Figure 1**. The shape of the samples allowed them to remain stuck in the drilled cylindrical hole, applying the stabilization criterion needed in the bone grafting procedure **[35 – 37]**. Sham holes remained empty as controls, with the aim of evaluating the spontaneous bone healing (**Figure 1(c)**). The fascia-periosteal flaps were sutured by 4.0 glycolide/L-lactide copolymer (Vicryl®, Ethicon, Johnson & Johnson, Livingston, UK) and the skin with 3.0 silk (Perma-hand® Silk Suture, Ethicon, Johnson & Johnson, Livingston, UK).

Post-operatively, single intramuscular injections of antibiotics (enrofloxacin, 10 mg/kg body weight) (Baytril 5%®, 50 mg/ml, , Bayer S.p.A., Milan, Italy) and analgesic (buprenorphine, 0.05 mg/kg body weight) (Temgesic®, Indivior Italia S.r.l., Milan, Italy) were given. The animals were housed with veterinary care and nutritional support in individual cages during the whole experimental period.

2.3. Samples' preparation and micro-radiography

The animals were sacrificed 60 days after surgical osteotomy with an intravenous injection of embutramide plus mebezonium iodide (0,3 ml/kg body weight) (Tanax® 50mg, MSD

Animal Health S.r.l. Italia, Segrate, Milan, Italy), under general anesthesia with a mixture of xylazine (4 mg/kg body weight) (Sedaxylan®, Dechra Veterinary Products Srl, Turin, Italy) and ketamine (30 mg/kg body weight)(Imalgene 1000®, Merial Italia SpA, Milan, Italy). The right and left femurs were disarticulated from the hip joint and the knee. Soft tissue was removed from the femurs by a dissector. Then, the femurs were put in formalin solution (10% buffered) at 4°C for 24 h. For histological preparation the specimens were washed for 1 h at 4°C in 0.1 M phosphate buffer pH 7.2.

X-ray imaging was performed on fixed femurs employing IVIS Lumina XMRS® imaging system (Perkin Elmer Italia S.p.A., Milan, Italy), used at low-energy (1-3 milligray (mGy) high-resolution (see **Figure 2**).

The femurs were dehydrated through an ascendant scale of ethyl alcohol, (70°, 80°, 90°, 99° and pure alcohol), treated for 10 h in a 1:1 pure alcohol/MMA (methylmetacrylate) moisture and then for one night in MMA only. Filtering solution was added for 24 h with 3 consecutive changes, then the samples were moved into a flatted bottom polyethylene container with the hermetically closed polymerizing solution and embedded in MMA. The container was maintained in a water bath at 4°C during the MMA polymerization process. After polymerization, histological sections were obtained by means of a bone microtome (REMET, Bologna, Italy).

Sections from the femur with implanted material were micro-radiographed, with a intraoral X-Ray digital imaging device (Vario^{DG}; Sirona Dental Systems S.r.l., Verona, Italy). The sections were cut to a thickness of 60-80-100 μm using diamond lap disk (LS2 Remet, Bologna, Italy) for histological dye and micro-radiography; a further set of thicker sections (500 μm) were prepared for observation in a scanning electron microscope (SEM, see next paragraph).

2.4. Histological analysis

The sections were stained in Stevenel's blue and counterstained with Van Gieson trichromic stain picro-fuchsin pro light microscopy. Samples preparation was specifically

carried out by immersion in Stevenel's blue stain, in a water bath at 60° C for 10 min, followed by rinsing in distilled water. Subsequently, the specimens were put in Van Gieson picro-fuchsin for 5 min at room temperature and then immersed in final rinse ethanol 100%. Poly-mount xylene was used for mounting. Finally, the following staining was obtained: purple/red to orange for mineralized bone, and shades of blue and green for non-mineralized osteoid **[38, 39].**

The sections were observed and analyzed in a light microscope (Nikon Eclipse 80, NIKON, Tokyo, Japan) connected to a personal computer with a software for morphometry (Nikon DS Fi1, Nikon, Tokyo, Japan). During the observation, particular attention was given to the interface between implant and bone, with the aim of determining the nature of the bone–implant interface and of searching for an eventual evidence of fibrous encapsulation, inflammatory reaction and bone contact.

500 μm thick sections were investigated by means of a SEM (ESEM Quanta 200, FEI Co., Eindhoven, The Netherland). The specimens were gold coated before observation. Local chemical analyses were carried out by X-ray energy dispersion spectroscopy, EDS (Inca, Oxford Instruments, UK).

3. Results

3.1. Comments on Surgery

One animal was sacrificed after 1 week of implantation because of fracture of one leg, probably due to the high weight of the animal itself. No complications were observed in the remaining animals. The sites of implantation appeared to be healed with no visible signs of infection, inflammation or adverse tissue reaction. Post-harvest radiographs were taken to confirm that the implants had been placed successfully, i.e. penetrating the cortex into the medullary canal of the femur, prior to gross reduction of the specimens. The sham-operated samples were not processed either for scanning electron or light microscopy.

3.2. Microradiography

An intraoperative view of the specimens during and immediately after implantation is shown in **Figures 1** and **2(a-d)**. All samples achieved the adequate stabilization required for osteointegration. Postoperative microradiographs reported in **Figure 2(e-h)** showed that the implanted rods were completely incorporated in the femur mid-shafts. The cortical bone layer healed over the implanted rods, covering them almost completely in all samples. Moreover, newly formed bone was present at the edge of the implants that overhanged in the marrow cavity, thus forming bone bridges that connect the implanted rods to the inner surface of medullary canal. In particular, all around the surface in the marrow cavity, the 45S5 rod showed a fine iso-denser layer compared to native femur bone (**Figure 2(e)**). The subsequent SEM analysis allowed to identify such layer as newly formed bone (see the following paragraphs). Also the BG_Ca/Mix rod, whose section has a triangular shape (**Figure 2(f)**), was surrounded by a fine iso-dense layer and a bridge of newly formed bone connected the edge of the implant to the wall of the marrow cavity (**Figure 2(f)**). A periosteal reaction **[40, 41]** with cortical hyperostosis was detectable over the outer left surface of the 80BG20HA section. In this case, several bone bridges came from the implant edges (**Figure 2(g)**). Finally, the 30BG70HA rod was well integrated in the femur cortex. Some aspects of incomplete healing produced irregularities of the outer cortex (i.e., empty spaces, see **Figure 2(h)**).

3.3. Sham hole

The spontaneous bone healing of sham holes in rabbits, after 60 days, has been well described by the scientific literature **[42]**, therefore the results dealing with the sham holes' healing have not been reported here in detail. Briefly, both the histology and the SEM investigation demonstrated the new bone formation within the defects. In particular, at the bone surface facing the bone marrow cavity (*i.e.* the endosteal surface), it was possible to note the difference in collagen fiber orientation between native mature cortical bone and the newly formed one. The thickness of the femur wall between the sham site and the native diaphysis was constant. The SEM observation revealed that the sham sites were

typically rich in cells, while the Harvesian canals were clearly detectable. It was possible to distinguish between the native cortical bone, which is more mineralized, and the newly formed one.

3.4. 45S5

Histology: As reported in **Figure 3(e, f)**, an intimate contact between newly formed bone and grafted implant was clearly observed. The newly deposited bone, in contact with all surfaces of the implant, was rich in cells. Collagen fibers organization of newly formed bone was parallel to the implant and perpendicular to the lamellar native bone (**Figure 3(e)**). No cracking and/or fracture of the grafted implant were observed. The interface surface was homogenous upon the grafted material, however some surface dissolution was detectable at higher magnification at the implant/bone interface. This *ground glass* aspect at the implant surface was ascribable to the formation of a hydroxyapatite (HCA) layer, with an underneath silica-gel like film (sgl, see the following paragraphs), which is the condition for achieving a stable bone tissue bonding (**Figure 3(e, f)**) **[21, 24, 43]**.

SEM: Bioactive bone-bonding mechanism is confirmed by SEM micrographs, reported in **Figures 3 and 4**. The formation of an HCA layer on the implant surface correspond to a *light grey line* in **Figure 3(a, b)**). Newly formed bone was clearly visible all around the implant. Some empty spaces were detectable in the outer cortex, but not directly in contact with the implant (**Figure 3(a)**). It is possible to observe the typical organization of collagen fibers of younger bone tissue, which is more irregular than that of native bone one (**Figure 3(b)**). It should be noted the partial dissolution of 45S5 under the superficial HCA layer at the bone/implant interface (**Figure 3(b)**). The bonding between implant and bone tissue was particularly stable and not interspersed with fibrous tissue. A non-homogeneous bone healing from a morphological point of view occurred in outer cortical layer of the femur mid-shaft, as some empty spaces were present; nevertheless, a newly bone layer was in direct contact with the implant by virtue of the material osteoconductivity (**Figure 3(a)**). It should be noted the presence of some cracks (see **Figure 3(a)** and **4(a)**).

The dissolution kinetics of the implant can be further analyzed by taking into account the EDS maps, which show the distribution of Si, P and Ca in the cross section of the implanted 45S5 (**Figure 7 (a, e, i, o)**). Si is representative of 45S5, while P and Ca are present both in 45S5, in HCA and in the bone. It should be noted a non-uniform dissolution of the implant, which is characterized by areas with higher Si or Ca content. On the contrary, the distribution of P in the implant is rather uniform. At the interface between implant and bone it is possible to detect some areas mainly composed by Ca and P, which are related to the formation of HAC.

3.5. BG_Ca/Mix

Histology: Newly formed bone was in strict contact with the implant, without any intervening fibrous layer. The interface between bone and implant was homogenous upon the grafted material, but extensive surface dissolution was detectable at higher magnification at the border of the implant/bone interface (**Figure 3(g, h)**). Indeed, the profile between implant/bone appeared quite irregular and undulated, and this fact can be ascribed to dissolution of the bioglass with concurrent formation of an HCA layer and an underneath sgl film, i.e. a layer rich in Si and poorer in alkaline and alkaline earth ions with respect to the original glass. This behavior was similar to the 45S5 one, although the sgl layer in BG_Ca/Mix sections appeared thinner with respect to the 45S5 ones (**Figure 3(g, e)**). It should be noted that the formation of silica gel is reported among the steps which lead to the conversion to HCA of the surface of bioactive glasses **[21]** in physiological environment and, subsequently, to the formation of a bonding between implanted bioglass and bone.

SEM: The implant showed good integration and high osteoconductivity, even in the portion that overhanged in the marrow cavity (**Figure 3(c)**). The boundary between newly formed bone and native one is evident, as well as the woven organization of the fibers in the former (**Figure 3(c)**). It should be noted that the superficial dissolution of the implant, which is clearly visible, is more homogenous with respect to the 45S5-derived ceramic here investigated. In **Figure 3(d)** it is possible to note the formation of a HCA layer on the

implant surface, which is observable as a *light grey line*, while the sgl film is the *dark grey band* surrounding the implant. The performance of BG_Ca/Mix in terms of osteoconductivity has been further compared to that of 45S5 in the micrographs of **Figure 4**. In particular, in the BG_Ca/Mix sample (**Figure 4(d)**) it is possible to note the formation of a sort of newly formed "bony bridge" which connects the implant and the native bone. Similar structures were not observable in 45S5 samples (see **Figure 4(c)**). Contrary to what has been previously said about 45S5 implants, the SEM investigation did not reveal the presence of cracks for BG_Ca/Mix samples. However, it is possible to note some residual porosity in the specimens (**Figure 3 (c, d)** and **Figure 4 (b, d)**).

The interface between BG_Ca/Mix implant and bone is investigated at higher magnification in **Figure 5**, where the results of the local chemical analyses carried out by EDS are reported as well. **Figure 5(a)** shows the different regions of the bioactive glass that have reacted with blood and bonded to bone: due to the ion exchange of K^+, Na^+ and Ca^{2+} from the BG_Ca/Mix with H^+ from the blood, a film rich in Si and with a lower content in alkaline and alkaline earth ions with respect to the original glass forms at the surface of the implant (see **Figure 5(f)**, such film has been identified as sgl in the previous paragraph), with a HCA film (**Figure 5(e)**) between this and the existing bone. In particular, new bone tissue was formed and it is progressively growing into the defect and into the marrow cavity area. This fact clearly indicates osteoconduction. These findings are analogous to those reported in Ref. **[44]**.

The EDS maps shown in **Figure 7 (b, f, l, p)** report an almost uniform distribution of Si in the implant, apart from the bone/implant interface, where it is possible to envisage the coexistence of HCA and sgl areas. The bone tissue revealed the presence of Si traces, arising from the dissolution of the adjoining glass. The almost uniform distribution of Ca along the cross section is indicative of the high Ca content in BG_Ca/Mix.

3.6. 80BG20HA

Histology: The interface between the implant and the bone was clear and linear (see **Figure 6(e, f)**). Newly deposited bone was in contact with the bioactive glass and rich in cells. Several osseous lacunae were suggestive of newly deposited bone and remodeling process. The refractive particle related to HA granules were disposed in aggregate, both on the interface and inside the implant (**Figure 6(e, f)**). A layer related to the dissolution of the glass phase, *pink-purple* colored in **Figure 6(e, f)** was detected at the surface of the implant. The edge between the newly deposited bone and the native bone was clearly observable, as the bony lamellae were parallel in the native trabecular bone, while woven bone is characteristic of young newly deposited tissue adjacent to the implant (**Figure 6(e)**).

SEM: SEM images, reported in **Figure 6(a, b)** showed that the newly formed bone tissue is in direct contact with the material; there are no empty spaces, on the contrary the newly deposited bone began the static osteogenesis starting from the implant material. The newly deposited bone all around the rod surface, which was overhanged in the medullary canal, documented an evident osteoconductive property of 80BG20HA (**Figure 6(a)**). Both the superficial dissolution of the implant and the bioactive bone-bonding mechanisms were evident: in this case, the HCA layer which formed on the implant surface correspond to *light grey line* in **Figure 6(b)**. Microcracking was visible at high magnification, but never on the bone/implant interface (**Figure 6(b)**). Finally, it should be noted the presence of several *light gray* stripes of bone interspersed in the *dark gray* newly formed bone, which documented an active bone remodeling with mineralization towards a lamellar bone tissue pattern (**Figure 6(b)**). The EDS maps reported in **Figure 7 (c, g, m, q)** showed the presence of both HA- and Si-rich areas. While the latter can be mainly associated to the glassy phase in 80BG20HA, the HA-rich areas, which correspond to *light grey* areas in **Figure 7(c)**, are ascribable to the calcium phosphate phase in the 80BG20HA composite and, to a lesser extent, to the HCA which formed at the implant/bone interface.

3.7. 30BG70HA

Histology: The rod was mechanically and partly disaggregated in particles during the implantation and by the subsequent contact with physiological fluids (see **Figure 6(g, h)**). Therefore, the interface between bone and material was markedly irregular and not linear, and the bone/implant contact was somewhere discontinuous. Some granules of the composite were dispersed in the area surrounding the implant. It should be noted the presence of newly deposited bone around such 30BG70HA particles.

SEM: SEM micrographs, reported in **Figure 6(c, d)** confirmed the histological findings. The material appeared to be highly fragmented in micro-granules and some of them were surrounded by new bone trabeculae (*white arrow*, **Figure 6(d)**). The bone/implant interface showed several wide gaps, while newly formed bone islands were developed incorporating granules of BG30HA70. A distinct layer of newly formed bone was present beyond disaggregated micro-granules and empty spaces (see **Figure 6(d)**). The porous structure of newly deposited bone, due to higher cellular density, is visible; on the contrary, native mature bone appeared in *light grey* due to higher mineralization. Newly formed bone was distinguishable all around the implant, however it was almost impossible to identify a precipitated HCA-layer surrounding the material. The results of the EDS analysis, reported in **Figure 5(b, g)**, showed the presence of Si, representative of the BG_Ca/Mix phase in the composite, only in the inner part of the implant, i.e. the region that has been less affected by the physiological fluids. Elsewhere the glass phase of the composite is almost dissolved. This fact is further confirmed by the results of the EDS maps reported in **Figure 7 (d, h, n, r)**, where it was difficult to identify the presence of Si, representative of the glass, at the bone/implant interface. The silicon traces are evenly spread both in the bone tissue and in the composite, which is rather fragmented.

4. Discussion

Based on previous investigations, the novel BG_Ca/Mix looks particularly promising, with respect to the widely used 45S5 Bioglass®, whenever a heat treatment is necessary for the

production of specific systems such as scaffolds or bioceramic composites. In fact, the main advantage of BG_Ca/Mix is its low tendency to crystallize. Besides reducing the bioactivity of the final system, it is reported that crystallization may also inhibit or slow down the sintering process, so the higher thermal stability of BG_Ca/Mix is expected to facilitate the production of fully dense bodies starting from glass powders. As a matter of fact, BG_Ca/Mix powders are able to consolidate at relatively low temperatures (about 800°C), almost preserving the amorphous nature of the glass and its bioactivity **[25]**. The same temperatures would be inadequate to sinter 45S5, which has been reported to reach a full densification only after thermal treatments between 1050°C and 1100°C **[45, 46]** which cause a wide crystallization of the final system with the formation of $Na_2Ca_2Si_3O_9$ and $Na_2CaSi_2O_6$ phases **[34, 45, 46]**.

Recent biocompatibility tests performed with murine osteocites and fibroblasts demonstrated the high osteoconductive potential of both BG_Ca/Mix sintered powders and of HA/BG_Ca-Mix composites **[28]**. Based on these encouraging results, it was conceivable that the produced materials could induce bone growth *in vivo* in an animal model. In this sense, the rabbit femur is suitable for the in vivo evaluation of osteoconduction of bioceramics **[47]**.

The second motivation of the present study is to compare the performances of BG_Ca/Mix and related HA-composites to 45S5 sintered powders, in order to identify possible advantages of the novel systems for the realization of products that requires a consolidation of the starting powders. In this sense, there is lack in the literature of works based on animal model dealing on both 45S5 sintered powders and on HA-based composites with silicate glasses as second phase, such as BG_Ca/Mix.

Bone healing at the interface with the bone substitute was observable for all the implants here studied, independently of the material composition. In particular, the materials presented evidence of osteoconduction. However, BG30HA70 looks rather different in terms of performance: in fact, after 2 month of implantation, the implant was rather disaggregated and newly deposited bone was not homogenously organized, but often spread in islands around the HA, which have not been reabsorbed. Integration partially

occurred, nevertheless several visible non mineralized spaces between implant and bone were specially detected by SEM. The spaces between BG30HA70 granules were locally filled by new woven bone. Therefore, it is possible to conclude that BG30HA70 showed the minor bone regeneration of the defect in comparison with remaining bone substitutes evaluated in the present study. This is mainly due to the high HA content of BG30HA70. In fact, several Authors demonstrated that, although HA is osteoconductive **[20, 48]**, HA implants have a slower bone apposition, integration and resorption compared to bioactive glasses and glass-ceramics **[49, 50]**. For example, implanted HA grafts are reported to remain within the body for extended periods of time with no signs of resorption **[51]**. The low reactivity and biodegradability in physiological environment of HA is ascribable to its close similarity between the mineral phase of bone. Therefore, it is not possible to exclude that a further bone apposition and healing could occur for BG30HA70 if implantation time would be longer. The disaggregation of BG30HA70, which is mainly due to its residual porosity after sintering **[28]**, could be exploited in the future for the realization of systems for controlled drug delivery.

45S5-derived glass-ceramics, BG_Ca/Mix and BG80HA20 were surrounded by newly formed bone, in direct contact with the material surface. Such materials did not show any intervening fibrous tissue: this aspect indicates good biocompatibility with consequent osseointegration. The gradual surface dissolution of the implants did not produce signs of inflammation at the interface between bone and material and it was not observed any implant cracking, thus moving away from similar studies based on animal models (see, for example, **[47]**). It is known that the direct bone bonding with the grafted materials depends on the bioactive nature of the interface **[52]**; in this sense, the osteoconduction ability of 45S5, BG_Ca/Mix and BG80HA20 was confirmed by the formation of a stable interface with the implant, which is characterized by the presence of a HCA film. Such film was not observable in BG30HA70 samples, where the newly deposited bone is distributed in discontinuous islands instead of in an almost continuous layer.

Generally speaking, regarding the specific performance of the investigated materials in terms of osteoconduction, it is possible to observe that BG_Ca/Mix samples were slightly higher osteoconductive than 45S5 derived glass ceramics, followed by BG80HA20 and BG30HA70. In particular, both BG_Ca/Mix and 45S5 allowed the bone osteoconduction over the rod surface that overhanged into the bone marrow cavity, but the newly formed bony layer was more appreciable in BG_Ca/Mix samples (see **Figure 4**). Moreover, although the apex of the rod that jutted out into the bone marrow cavity was close to the endosteal surface both in 45S5 and in BG_Ca/Mix samples, nevertheless in BG_Ca/Mix the newly formed bone connected the rod to the inner cortical bone, thus making a sort of "bony bridge" between the graft and the bone tissue adjacent to the bone marrow cavity (see **Figure 4(d)**); it should be taken in mind that in long bones, such as femurs, the bone marrow cavity is devoid of bone. Similar "bony bridges" were not present in 45S5 samples. This fact may be partly ascribed to the amorphous nature of BG_Ca/Mix, while 45S5 – as previously discussed – is partially crystallized in response to the thermal treatment which was employed to sinterize the starting glass powders, and the biological performance of 45S5 is expected to be affected by such crystallization. In addition, several cracks were observable in 45S5. In this context, it is reported by the literature that the partial crystallization of the glass could lead to implant instability, since the residual amorphous phase is degraded preferentially by organic fluids **[24, 53]**. This fact could be confirmed by the EDS maps here presented (**Figure 7**), where 45S5 is characterized by the presence of areas with higher Si or Ca content, thus indicating the potential non uniform dissolution of the implant. It is important to note that in biomedical applications a non-uniform dissolution of the implant should be avoided, since it can lead to the formation of non-uniform stresses along the graft and to its pre-mature mechanical failure. In this context, no cracks were observed, after 60 days of implantation, in the almost amorphous BG_Ca/Mix.

5. Conclusions

In this work, for the first time, a set of novel sintered bodies for bone tissue repair have been tested *in vivo* in an animal model. The samples were implanted bilaterally in the midshafts rabbit femurs and harvested after 8 weeks. The recently developed BG_Ca/Mix bioactive glass and two HA/BG_Ca-Mix composites with an increasing content of HA were considered. In addition, 45S5 sintered powders were implanted and used as a term of comparison. The preliminary findings reported in the present study demonstrated the high osteoconductivity of BG_Ca/Mix, which retained its amorphous nature despite thermal treatment employed to sinterize the starting glass powders. The osteoconductive ability of BG_Ca/Mix is slightly higher than that of 45S5 glass-ceramics, followed by that of BG80HA20 and BG30HA70 samples. However, the 45S5 specimens after 8 weeks of implantation were locally cracked: this fact may be ascribed to the partial crystallization of 45S5, as the residual glass phase was probably degraded preferentially by the physiological fluids. On the contrary such cracks, which could lead to implant instability and unsuitable mechanical performance **[24, 53]**, were not observed in BG_Ca/Mix. Morever, it should be noted that the densification of BG_Ca/Mix powders requires lower temperatures with respect to 45S5, therefore such novel bioactive glass looks particularly promising also from an economical point of view, whenever a thermal treatment is required for the production of specific systems, such as scaffolds or composites. In this context, since the osteoconductivity of BG80HA20 composites has been here demonstrated, it will be interesting to investigate the *in vivo* biodegradation rate of such systems after longer implantation times and to further vary the volume fractions of the two constituent phases, aiming to obtain systems with degradation rate tailored for a given clinical application. Finally BG30HA70, i.e. the composite richer in HA, looked fragmented after implantation, with the formation of novel bone tissue adjacent to HA particles. In this sense, the disaggregation of BG_Ca/Mix composites with an high content of HA could be exploited in the future for the realization of systems for controlled drug delivery.

6. Acknowledgments

Authors would like to thank Dr. Elvis Federzoni, DDS for his technical assistance in x-ray imaging acquisition.

7. References

1. L.L. Hench, J.M. Polack. Third-generation biomedical materials. Science 295 (2002) 1014–7.
2. X.J. Loh, E. Ye. Polymeric Hydrogels and Nanoparticles: A Merging and Emerging Field. Australian Journal of Chemistry 66 (2013) 997–1007.
3. Q.Q. Dou, C.P. Teng, E. Ye, X.J. Loh. Effective near-infrared photodynamic therapy assisted by upconversion nanoparticles conjugated with photosensitizers. Int J Nanomedicine 10 (2015) 10, 419-32.
4. K .Huang, Q. Dou, X.J. Loh. Nanomaterial mediated optogenetics: opportunities and challenges. RSC Adv. 6 (2016) 60896–60906.
5. Z. Li, E. Ye, David, R. Lakshminaravanan, X.J. Loh. Recent Advances of Using Hybrid Nanocarriers in Remotely Controlled Therapeutic Delivery. Small 12 (2016) 4782-4806.
6. X.J. Loh, T.C. Lee, Q. Dou, G.R. Deen. Utilising inorganic nanocarriers for gene delivery. Biomater Sci 4 (2016) 70–86.
7. C. Dhand, N. Dwivedi, X.J. Loh, A.N.J. Ying, N.K. Verma, R.W. Beuerman, R. Lakshminarayanan, S. Ramakrishna. Methods and strategies for the synthesis of diverse nanoparticles and their applications: a comprehensive overview. Rsc Advances 5 (2015) 105003-105037.
8. P. Gentile, D. Bellucci, A. Sola, C. Mattu, V. Cannillo, G. Ciardelli. Composite scaffolds for controlled drug release: role of the polyurethane nanoparticles on the physical properties and cell behaviour. Journal of the Mechanical Behavior of Biomedical Materials 44 (2015) 53-60.
9. E. Ye, M.D. Regulacio, S.Y. Zhang, X.J. Loh, M.Y. Han. Anisotropically branched metal nanostructures. Chem. Soc. Rev. 44 (2015) 6001–17.

10. E. Ye, M.D. Regulacio, M.S. Bharathi, H. Pan, M. Lin, M. Bosman, K.Y. Win, H. Ramanarayan, S.Y. Zhang, X.J. Loh, Y.W. Zhang, M.Y. Han. An experimental and theoretical investigation of the anisotropic branching in gold nanocrosses. Nanoscale. 8 (2016) 543-52.

11. H. Lu, Y. Liu, J. Guo, H. Wu, J. Wang, G. Wu. Biomaterials with anticterial and osteoinductive properties to repair infected bone defects. Int. J. Mol. Sci. 17 (2016) 334.

12. Q. Dou, X. Fang, S. Jiang, P.L. Chee, T.C. Lee, X.J. Loh. Multi-functional fluorescent carbon dots with antibacterial and gene delivery properties. RSC Adv**.** 5 (2015) 46817-46822.

13. A. Sola, D. Bellucci, V. Cannillo. Functionally graded materials for orthopaedic applications - an update on design and manufacturing. Biotechnology Advances 34 (2016) 504–531.

14. L. Altomare, D. Bellucci, G. Bolelli, B. Bonferroni, V. Cannillo, L. De Nardo, R. Gadow, A. Killinger, L. Lusvarghi, A. Sola, N. Stiegler. Microstructure and in-vitro behaviour of 45S5 bioglass coatings deposited by High Velocity Suspension Flame Spraying (HVSFS). J. Mater. Sci. Mater. Med. 22 (2011) 1303–1319.

15. H.C. Guo, E. Ye, Z. Li, M.Y. Han, X.J. Loh. Recent progress of atomic layer deposition on polymeric materials. Mater Sci Eng C Mater Biol Appl 70 (2017) 1182-1191.

16. X. Yu, X. Tang, S.V. Gohil, C.T. Laurencin. Biomaterials for bone regenerative engineering. Adv. Healthc. Mater. 4 (2015) 1268–85.

17. D. Bellucci, V. Cannillo, A. Sola. A new highly bioactive composite for scaffold applications: a feasibility study. Materials 4 (2011) 339–354.

18. D. Bellucci, A. Sola, V. Cannillo. Hydroxyapatite and tricalcium phosphate composites with bioactive glass as second phase: State of the art and current applications. J. Biomed. Mater. Res. Part A 104A (2016) 1030–1056.

19. S. Samavedi, A.R. Whittington, A.S. Goldstein. Calcium phosphate ceramics in bone tissue engineering: A review of properties and their influence on cell behavior. Acta Biomater. 9 (2013) 8037–8045.

20. Hydroxyapatite (HAp) for biomedical applications, In "Woodhead Publishing Series in Biomaterials: Number 95", 1st Edition, Edited by Michael Mucalo, Woodhead Publishing, Kidlington, UK, 2015.

21. L.L. Hench. Bioceramics: From concept to clinic. J. Am. Ceram. Soc. 74 (1991) 1487–1510.

22. A.A. Gorustovich, J.A. Roether, A.R. Boccaccini. Effect of bioactive glasses on angiogenesis: a review of in vitro and in vivo evidences. Tissue Eng. Part B Rev. 16 (2010) 199-207.

23. V. Miguez-Pacheco, L. L. Hench, A. R. Boccaccini. Bioactive glasses beyond bone and teeth: Emerging applications in contact with soft tissues. Acta Biomater. 13 (2015) 1–15.

24. J. R. Jones. Reprint of: Review of bioactive glass: from Hench to hybrids. Acta Biomater. 23 (2015) S53-82.

25. D. Bellucci, A. Sola, V. Cannillo. Low temperature sintering of innovative bioactive glasses. J. Am. Ceram. Soc. 95 (2012) 1313–1319.

26. P. Gentile, D. Bellucci, A. Sola, C. Mattu, V. Cannillo, G. Ciardelli. Composite scaffolds for controlled drug release: role of the polyurethane nanoparticles on the physical properties and cell behaviour. J. Mech. Behav. Biomed. 44 (2015) 53-60.

27. O. Bretcanu, X. Chatzistavrou, K. Paraskevopoulos, R. Conradt, I. Thompson, A. R. Boccaccini. Sintering and crystallisation of 45S5 Bioglass® powder. J. Eur. Cer. Soc. 29 (2009) 3299-3306.

28. D. Bellucci, A. Sola, A. Anesi, R. Salvatori, L. Chiarini, V. Cannillo. Bioactive glass/hydroxyapatite composites: Mechanical properties and biological evaluation. Mater. Sci. Eng. C 51 (2015) 196–205.

29. G. Bolelli, D. Bellucci, V. Cannillo, R. Gadow, A. Killinger, L. Lusvarghi, P. Müller, A. Sola. Comparison between Suspension Plasma Sprayed (SPS) and High Velocity

Suspension Flame Sprayed (HVSFS) bioactive coatings, Surf. Coat. Tech. 280 (2015) 232–249.

30. D. Bellucci, L. Desogus, S. Montinaro, R. Orrù, G. Cao, V. Cannillo. Innovative hydroxyapatite/bioactive glass composites processed by spark plasma sintering for bone tissue repair. J Eur Ceram Soc 37 (2017) 1723–1733.

31. J. Kolmas, A. Jaklewicz, A. Zima, M. Bućko, Z. Paszkiewicz, J. Lis, A. Ślósarczyk, W. Kolodziejski. Incorporation of carbonate and magnesium ions into synthetic hydroxyapatite: the effect on physicochemical properties. J. Mol. Struct. 987 (2011) 40–50.

32. D. Bellucci, A. Sola, R. Salvatori, A. Anesi, L. Chiarini, V. Cannillo. Sol-gel derived bioactive glasses with low tendency to crystallize: synthesis, post-sintering bioactivity and possible application for the production of porous scaffolds. Mater. Sci. Eng. C 43 (2014) 573–586.

33. L.L. Hench. The story of Bioglass®. J. Mater. Sci. Mater. Med. 17 (2006) 967–978.

34. D. Bellucci, V. Cannillo, A. Sola, F. Chiellini, M. Gazzarri, C. Migone. Macroporous Bioglass®-derived scaffolds for bone tissue regeneration. Ceram. Int. 37 (2011) 1575–1585.

35. F. J. Hornicek, M. C. Gebhardt, W.W. Tomford, J.I. Sorger, M. Zavatta, J.P. Menzner, H. J. Mankin. Factors affecting nonunion of the allograft-host junction. Clin. Orthop. Relat. Res. 382 (2001) 87–98.

36. K.Y. Lin, S.P. Bartlett, M.J. Yaremchuk, M. Fallon, R.F. Grossman, L.A. Whitaker. The effect of rigid fixation on the survival of onlay bone grafts: an experimental study. Plast Reconstr Surg. 86 (1990) 449–56.

37. J. Jensen , E. Krantz, E. Simonson, S. Sidet-Pedersen. Reconstruction of the severely resorbed maxilla with bone grafting and osseointegrated implants: a preliminary report. J Oral Maxillofac Surg 48 (1990) 27–32.

38. D.A. Deporter, P.A. Watson, R.M. Pilliar, A.H. Melcher, J. Winslow, T.P. Howley, P. Hansel, C. Maniatopoulos, A. Rodriguez, D. Abdulla, et al. A histological

assessment of the initial healing response adjacent to porous-surfaced, titanium alloy dental implants in dogs. J Dent Res. 65 (1986) 1064-70.

39. L. Jahangiri, R. Hessamfar, J.L. Ricci. Partial generation of periodontal ligament on endosseous dental implants in dogs. Clin Oral Implants Res. 16 (2005) 396–401.

40. K. Muramatsu, A.T. Bishop. Cell repopulation in vascularized bone grafts. J Orthop Res. 20 (2002) 772–8.

41. O.R. Ozerdem, R. Anlatici, T. Bahar, F. Kayaselçuk, O. Barutçu, I. Tuncer, O. Sen. Roles of periosteum, dura, and adjacent bone on healing of cranial osteonecrosis. J Craniofac Surg. 14 (2003) 371–9; discussion 380–2.

42. D. E. Ashhurst. The influence of mechanical conditions on the healing of experimental fractures in the rabbit: a microscopical study. Philos Trans R Soc Lond B Biol Sci 313 (1986) 271–302.

43. G. Kaur, O.P. Pandey, K. Singh, D. Homa, B. Scott, G. Pickrell. A review of bioactive glasses: Their structure, properties, fabrication and apatite formation. J Biomed Mater Res A. 102 (2014) 254-74.

44. M. D. O'Donnell. Melt-Derived Bioactive Glass Bio-Glasses: An Introduction (2012) 2 ed JR Jones and A G Clare (Chichester, UK: John Wiley & Sons, Ltd) 13-27 chapter.

45. L. Lefebvre, J. Chevalier, L. Gremillard, R. Zenati, G. Thollet, D. Bernache- Assolant, A. Govin. Structural Transformations of Bioactive Glass 45S5 With Thermal Treatments. Acta Mater. 55 (2007) 3305–13.

46. Q.Z. Chen, I.D. Thompson, A.R. Boccaccini. 45S5 Bioglass-derived glass-ceramic scaffolds for bone tissue engineering. Biomaterials 27 (2006) 2414–2425.

47. S. Bandyopadhyay-Ghosh, P.E. Faria, A. Johnson, D.N. Felipucci, I.M. Reaney, L.A. Salata, I.M. Brook, P.V. Hatton. Osteoconductivity of modified fluorcanasite glass-ceramics for bone tissue augmentation and repair. J Biomed Mater Res A 94 (2010) 760–8.

48. M. Jarcho, J.F. Kay, K.I. Gumaer, R.H. Doremus, H.P. Drobeck. Tissue, cellular and subcellular events at a bone-ceramic hydroxylapatite interface. J Bioeng. 1 (1977) 79-92.

49. N. Ikeda, K. Kawanabe, T. Nakamura. Quantitative comparison of osteoconduction of porous, dense A-W glass-ceramic and hydroxyapatite granules (effects of granule and pore sizes). Biomaterials 20 (1999) 1087-1092.

50. H. Oonishi, L.L. Hench, J. Wilson, F. Sugihara, E. Tsuji, S. Kushitani, H. Iwaki. Comparative bone growth behavior in granules of bioceramic materials of various sizes (1999). J Biomed Mater Res 44 (1999) 31-43.

51. P. Proussaefs, H.S. Olivier, J. Lozada. Histologic evaluation of a 12-year-old threaded hydroxyapatite-coated implant placed in conjunction with subantral augmentation procedure: a clinical report. J. Prosthet. Dent. 92 (2004) 17-22.

52. An Introduction to Bioceramics. Edited by: L.L. Hench. 2nd Edition World Scientific Publishing (2013).

53. O. Peitl, G.P. LaTorre, L.L. Hench. Effect of crystallization on apatite-layer formation of bioactive glass 45S5. J. Biomed. Mater. Res. 30 (1996) 509–14.

8. Figure captions

Figure 1. Intra-operative pictures of hole drilling in rabbit midshaft (a, b). Bioceramic rods were positioned in the holes as shown in (c); in particular, the diagram reported in (c) described the proximal and distal anatomic orientation of the rabbit left femur: the sample 1 is more proximally placed compared to the sample 2. A micro-radiography performed on a postharvest rabbit femur is shown in (d).

Figure 2. Intraoperative view of the bioceramics specimens immediately after implantation (a-d). Thanks to hole calibration related to specific rods' dimension, all samples achieved the stabilitation required for osteointegration. Cross-sectional micro-Rx of rabbit femurs in the site of rods' implantation, acquired after harvesting, are reported in (e-f).

Figure 3. SEM and histological (*Van Gieson/Stevenel's blue stain*) sections of 45S5 (a, b, e, f) and BG_Ca/Mix (c, d, g, h).

Figure 4. SEM sections of 45S5 (a, c) and BG_Ca/Mix (b, d).

Figure 5. The interface between bone and BG_Ca/Mix implant (a), and the 30BG70HA implant (b); (c–g): results of the EDS analysis performed on the areas reported in (a) and (b).

Figure 6. SEM and histological (*Van Gieson/Stevenel's blue stain*) sections of 80BG20HA (a, b, e, f) and 30BG70HA (c, d, g, h). The white arrow in (d) indicates an island of new formed bone which developed around disaggregated micro-granules of 30BG70HA.

Figure 7. SEM micrographs of the implanted materials' cross sections (a-d) and corresponding EDS maps showing the distribution of Si (e-h), which is representative of the glass phase in the produced materials, P (i-n) and Ca.

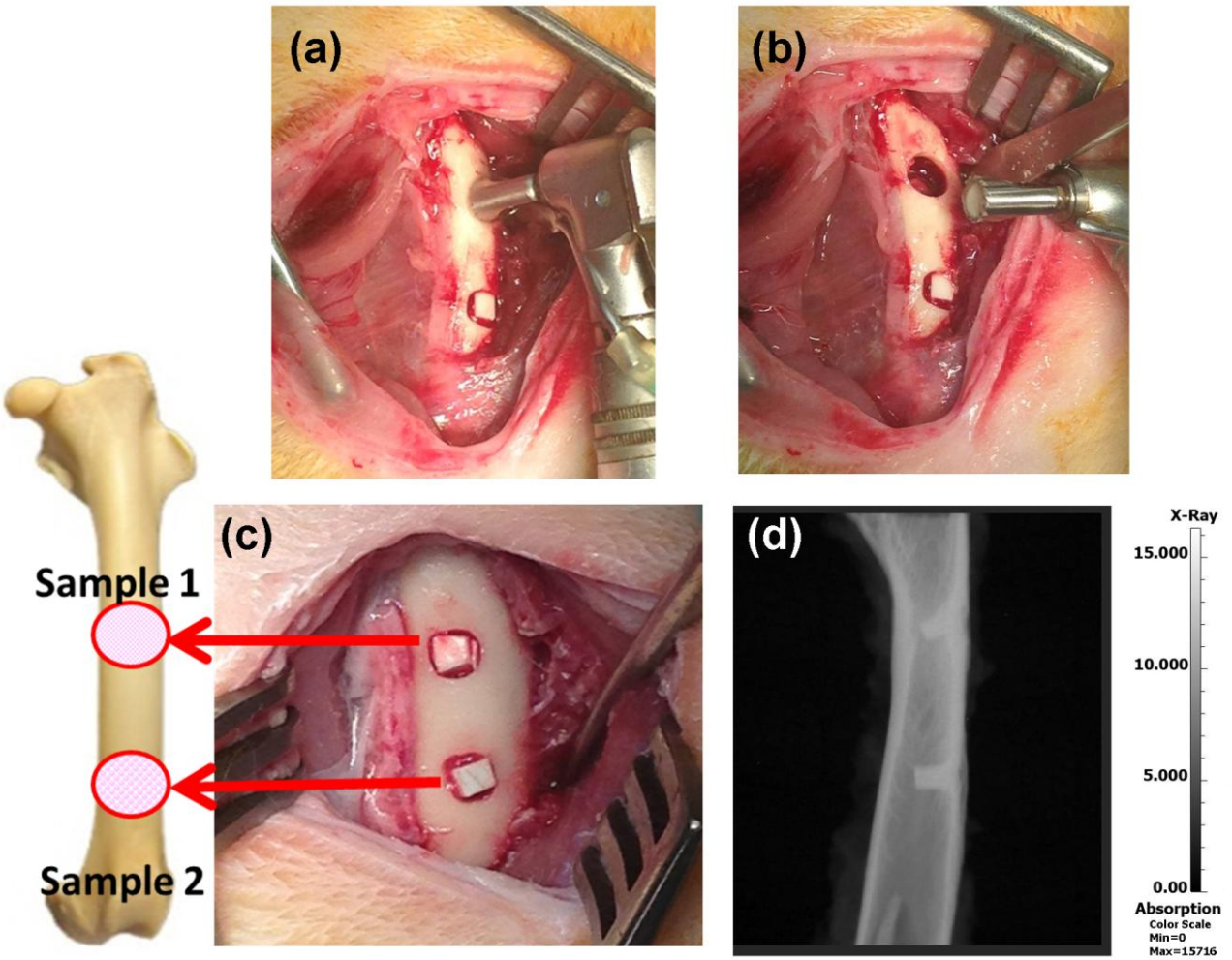

Fig. 1

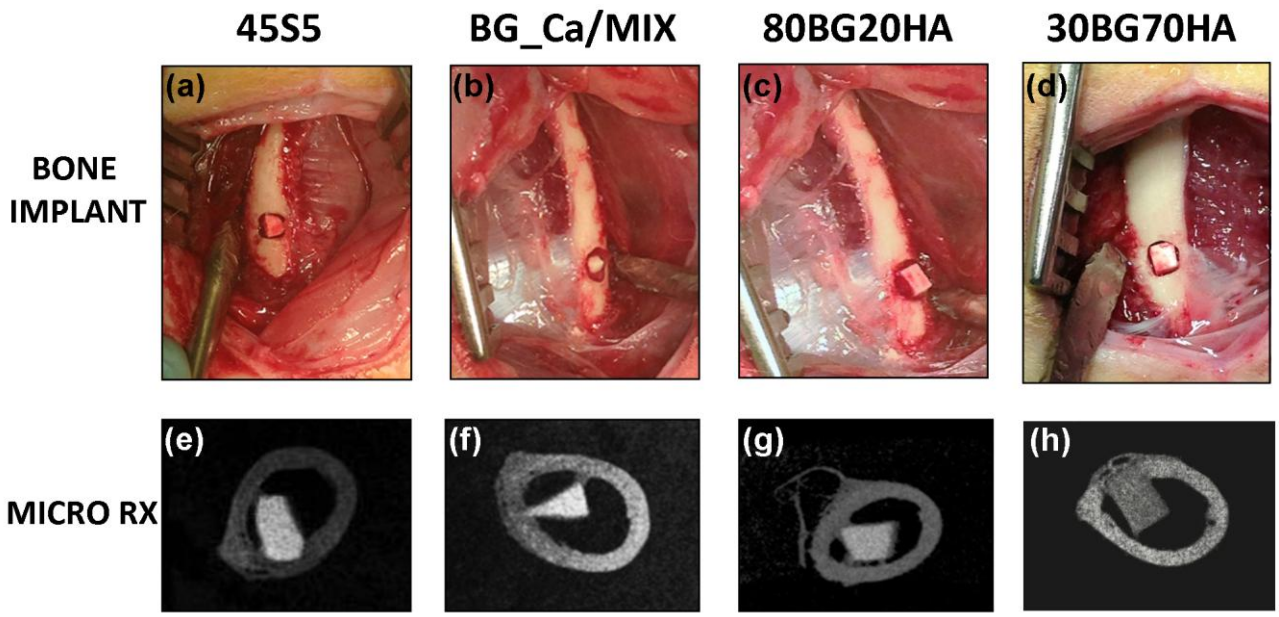

Fig. 2

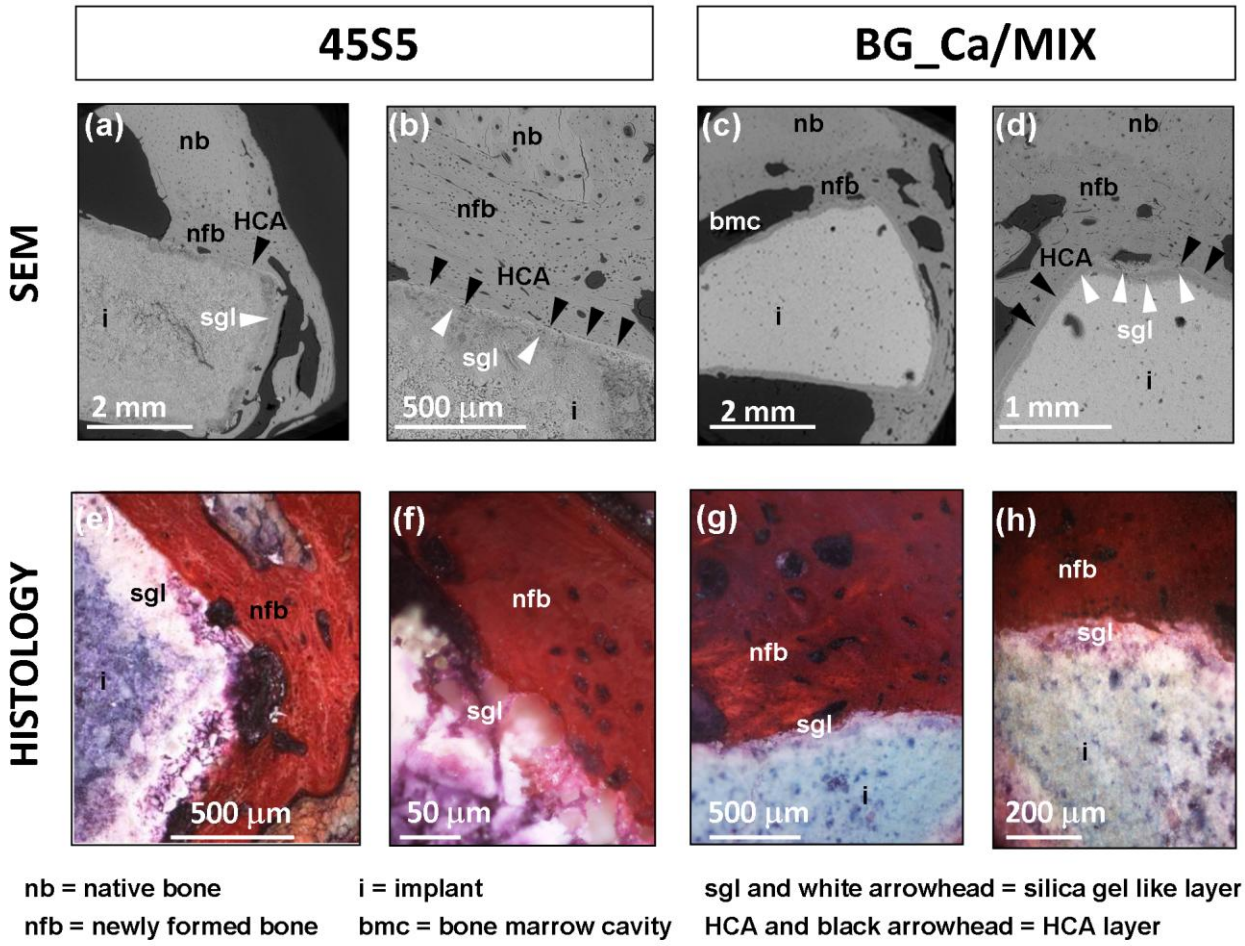

Fig. 3

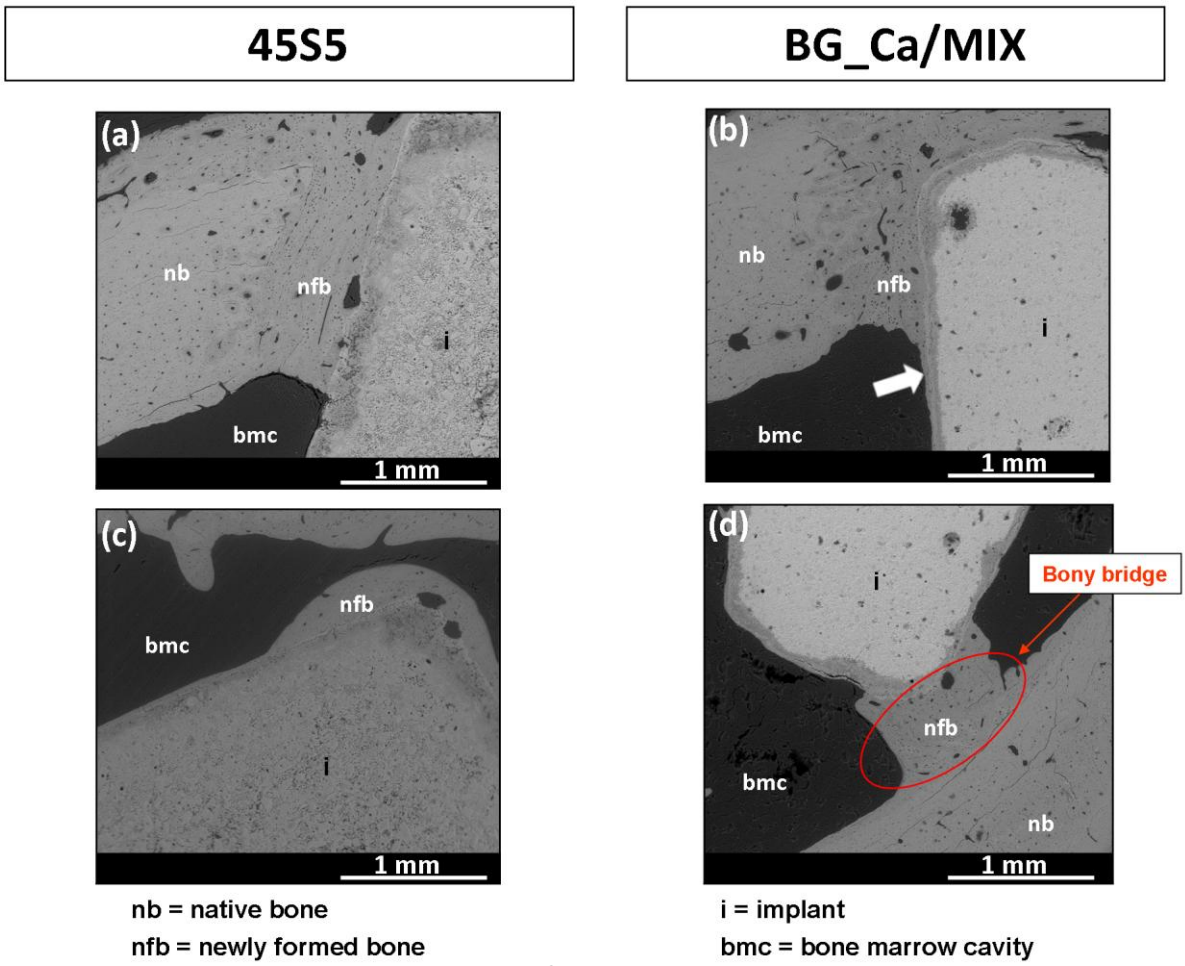

Fig. 4

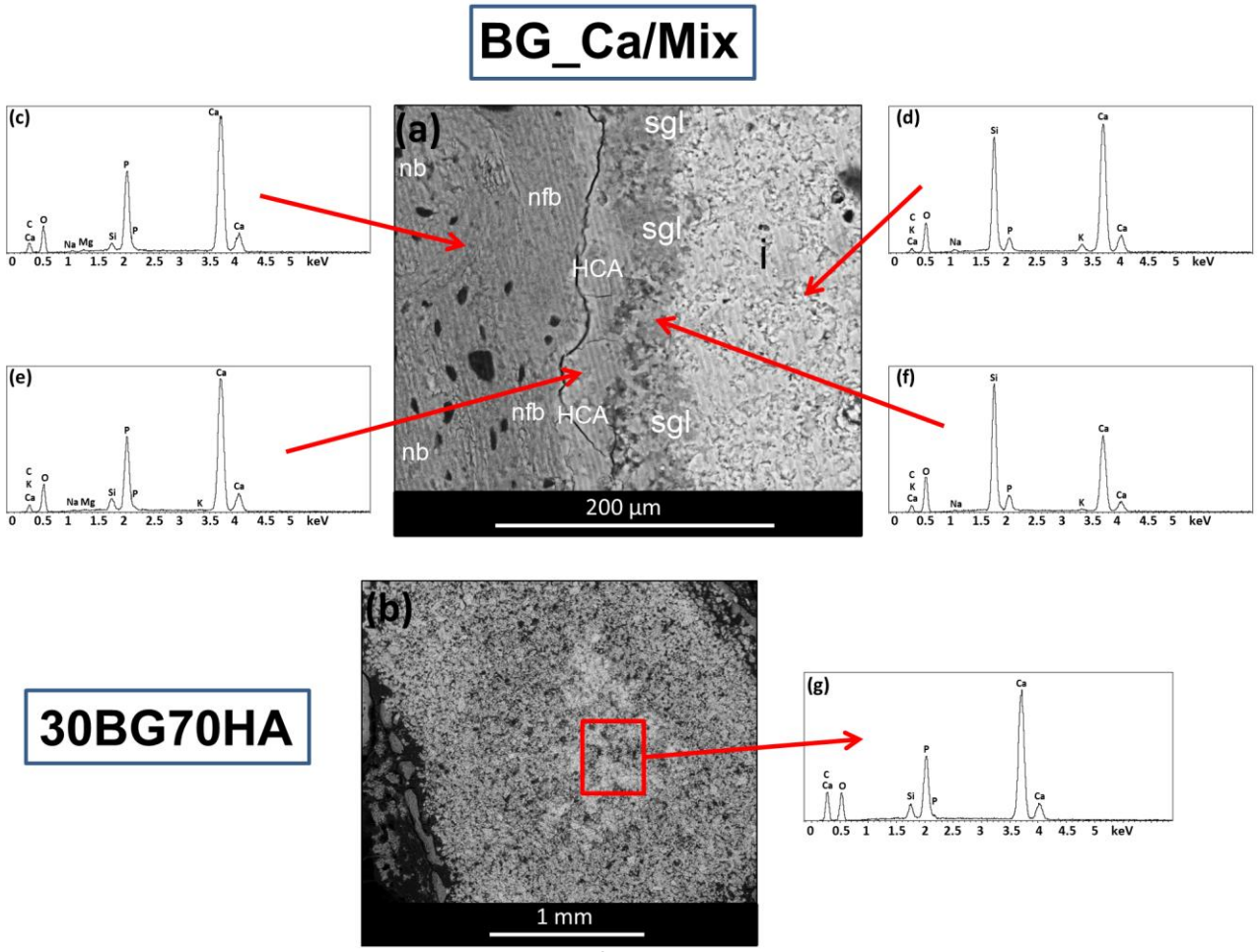

Fig. 5

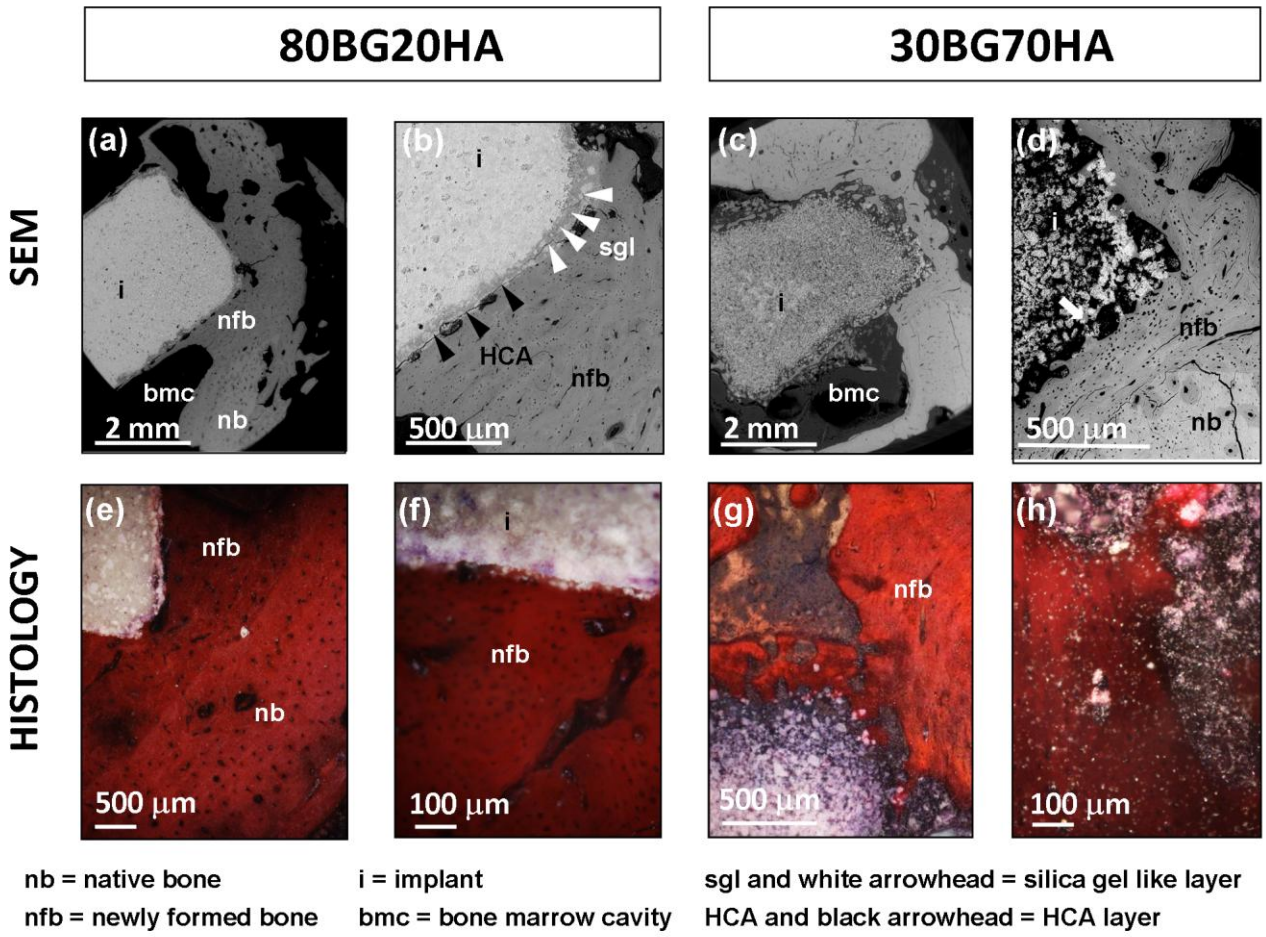

Fig. 6

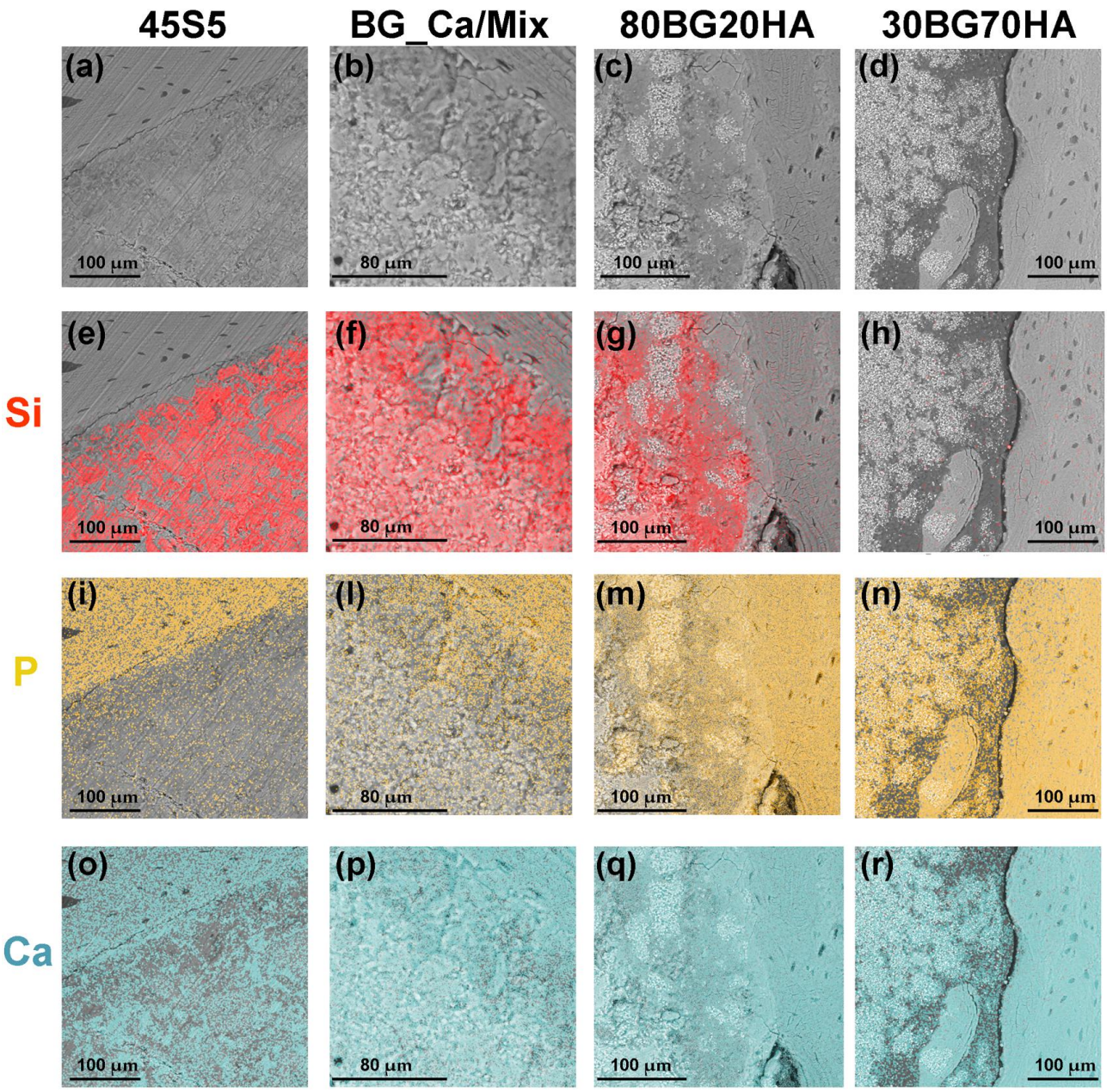

Fig. 7

Highlights

- New sintered bodies (a bioglass and two composites) were tested in vivo in rabbits
- 45S5 Bioglass® sintered powders were implanted and used as a term of comparison
- Compared to 45S5, the new glass preserved its amorphous phase after sintering
- The new bioglass is slightly higher osteoconductive than 45S5 glass-ceramics
- The performance of the new bioglass is better also in terms of implant's stability